PCCP

PAPER

View Article Online
View Journal | View Issue

Cite this: *Phys. Chem. Chem. Phys.*, 2021, **23**, 24905

Freezing efficiency of feldspars is affected by their history of previous freeze–thaw events†

Elzbieta Pach and Albert Verdaguer *

Received 7th June 2021,
Accepted 20th October 2021

DOI: 10.1039/d1cp02548a

rsc.li/pccp

Among the different aerosol mineral particles that contribute to induce ice nucleation (IN) in the troposphere, feldspars have been identified as the most active. Nevertheless, which surface properties make some feldspars more efficient than others, *i.e.* able to induce IN at higher temperatures, is still unclear. In addition to that, surface properties of such materials can change as they are exposed to a variety of environmental conditions while traveling through the troposphere. Here, freezing temperature of water droplets deposited on feldspar minerals has been measured as a function of consecutive freeze–thaw cycles. We found an increase of the freezing temperature for the initial cycles followed by approximately constant freezing temperature for consecutive cycles. We call this a "history effect". This effect is more evident for samples aged in standard room conditions and it disappears if the sample is exposed to oxygen plasma. Oxygen plasma generates OH groups at the surface, facilitating IN and cleans the surface from organic contamination, unblocking pores at the surface, believed to be the most active IN sites on feldspars. A similar process is suggested to happen during the history effect, when consecutive freeze–thaw events unblock IN sites.

Introduction

Ice plays a key role in many phenomena happening at the surface of earth, from climate to geology and life. Almost a decade ago, ten basic questions about ice and snow were considered essential for predicting earth's future.[1] The first of those questions was to understand the processes by which ice is formed in the troposphere; ice nucleation (IN). IN from liquid water can happen through homogeneous or heterogeneous routes. If liquid water is cooled below 0 °C, it stays in a supercooled liquid state until IN happens spontaneously (homogeneous nucleation) or is induced by a substrate (heterogeneous nucleation).[2] Homogeneous nucleation happens at temperatures much lower than the ice melting point. Water can remain in a supercooled state at temperatures as low as −38 °C. Heterogeneous nucleation happens at higher temperatures than homogeneous nucleation, thus the presence of substrates in contact with water enhances IN. In the atmosphere, heterogeneous IN is initiated by aerosol particles, dust, pollen, *etc.*[3] Among the different aerosol particles that contribute to induce IN in the troposphere, K-rich feldspars have been identified as the most active particles amid ice-nucleating minerals.[4]

Based on classical nucleation theory, when IN is triggered and an ice embryo is formed, the critical size for ice embryo to be able to initiate the freezing of surrounding water is at the nanoscale level[5,6] thus heterogeneous nucleation is induced in nanometric–size areas of the surface. This theory has been supported by IN observed in mesopores[7] and there are clear evidences that heterogeneous IN on minerals such as feldspars occurs at a small number of specific sites on the surface.[8,9] These findings reveal why it is so challenging to have a deep understanding of the factors and properties of a surface that can drive heterogeneous nucleation; tiny variations in topography or chemical composition at the nanoscale can generate strong heterogeneities in the ice-nucleation efficiency from different sites of a surface. Topographically, it has been observed that microtextures,[10] related to phase separation into Na- and K-rich regions, showed exceptional ice nucleating abilities.[11] In our previous studies, we observed, by environmental scanning electron microscopy (E-SEM), that IN on feldspars occurs mainly inside pores exposed at the surface.[12] From the chemical point of view, the different arrangement of OH groups at the surface of feldspars seems to be responsible for their ice-nucleation efficiency.[9,13] Since IN is very sensitive to the surface properties of the substrate it is important to know, beyond intrinsic surface properties of the materials, how surface properties change while the substrate is exposed to environment and to freeze–thaw events as particles travel in the troposphere. To our knowledge, not a lot of studies have been devoted to the study on how the history of such surfaces affects its IN properties.[14–18] Nevertheless, it is known that contact of the surface with water at low temperatures, previous to a freezing event, can induce a phenomena called pre-activation of ice-nucleating particles.[19–21]

Institut de Ciència de Materials de Barcelona ICMAB-CSIC, Campus de la UAB, E-08193 Bellaterra, Spain. E-mail: averdaguer@icmab.es

† Electronic supplementary information (ESI) available. See DOI: 10.1039/d1cp02548a

In a pre-activation scenario, the ability of a material for IN is enhanced by a temporary exposition to low temperatures in the presence of water vapour. During the exposition, pores and surface cracks of the particles fill with ice that would survive at higher temperatures and later act as more efficient ice-nucleation sites. Differences in the IN ability depending on aging of the surface were also pointed out in some E-SEM experiments with no deep investigation on the causes.[9] Modification of feldspar surface morphology by chemically inducing the formation of cracks also revealed an increase of the ice-nucleation activity of the surface.[22] Thus, beyond intrinsic properties of the material, history of the surface of the material should be taken into account to determine its ice-nucleation abilities. Here, we report how previous history of freeze–thaw events affects freezing of water droplets in contact with surfaces of feldspar minerals created by cleavage. We found that the freezing temperature of such droplets depends on previous freeze–thaw events experienced by the same droplet and surface. We observed that these temperatures increased with every freeze–thaw event until a stable regime was reached. This behaviour also strongly depends on aging of the sample at room conditions and can be suppressed by exposing the surface to oxygen plasma before the first freezing experiment.

Experimental

A LTS120E Linkam chamber (Linkam Scientific Instruments, Surrey, UK) was assembled on the stage of an Olympus BX41M-LED optical microscope to control both the temperature and the environment of the sample. The optical microscope was equipped with 10x, 20x and 50x long working distance objectives (LMPLFLN10X, SLMPLN20X and SLMPLN50X, Olympus) and a Hamamatsu ORCA-Flash 4.0 Digital CMOS C11440 high-speed camera (Hamamatsu Photonics, Japan). The LTS120E chamber was equipped with a Peltier cooling stage able to cool down to −25 °C with a platinum resistor sensor embedded close to the surface for accurate temperature measurements (±0.1 °C error in temperature measurements). The experimental set up allows to monitor and record the freezing process of water at high speed with up to 8000 frames per second.[8,23] Frames are recorded simultaneously with time and sample temperature, thus the temperature at which freezing begins can be determined unambiguously from image analysis. Freezing of water was examined on three different K-feldspar samples. The feldspars correspond to: GREEN, amazonite from Minas Gerais, Brazil with a microcline structure and albite inclusions, ORANGE from Hyderabad, India with a microcline structure and GOLDEN, orthoclase sample from Mt. Malosa, Malawi (Fig. 1). The minerals were cut forming slices of 5 × 10 mm and 200 μm thickness. Pictures of the minerals and the cuts performed are shown in Fig. 1. GREEN and ORANGE feldspars were cut along the natural cleavage planes observed in the minerals which were found to correspond to the (100) plane for GREEN (following albite inclusions direction[24]) and the (001) for ORANGE. Additional cuts were performed on both samples perpendicular to those

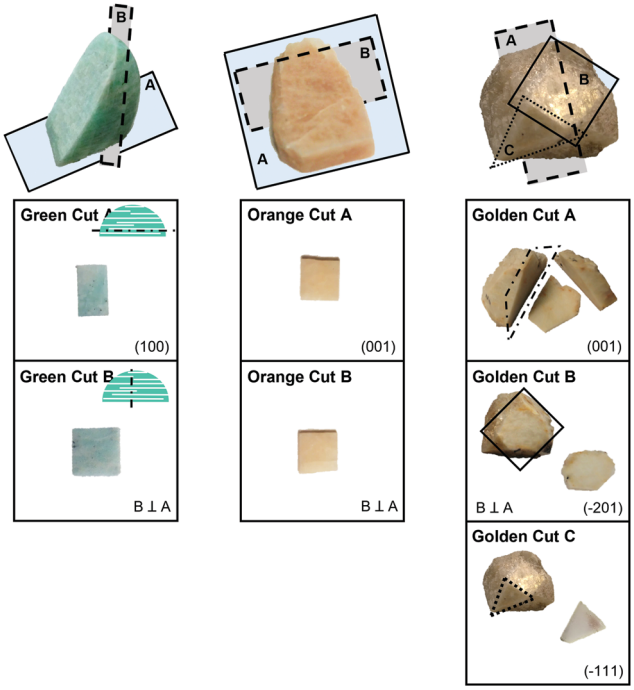

Fig. 1 Pictures of the cuts performed on the three different feldspar minerals following the main crystallographic directions shown by the crystals and perpendicular to them. From left to right: GREEN, ORANGE and GOLDEN. Indexing of the crystallographic planes was based on the X-ray diffraction (XRD) patterns (Fig. S1, ESI†).

planes. The GOLDEN sample, which is a baveno twin, was cut along (001) plane (cut A) and along two of the exposed natural cleavage planes, (−201) and (−111) (cut B and C, respectively). In this way, seven different slices corresponding to three different samples and 2 to 3 different orientations for each feldspar were obtained. Using environmental scanning electron microscopy (E-SEM) IN on the slices was tested. Ice crystals formed on the surface were oriented following the different crystal orientations exposed as previously reported (see Fig. S2, ESI†).[9,23] Every slice was then cut into four to six pieces. Experiments were repeated on these pieces for reproducibility tests.

In the freeze–thaw experiments a single piece of feldspar was placed on the Peltier stage, a droplet of 10 μl of MilliQ water was placed on the piece and then successive freeze–thaw cycles of the droplet were performed. A cycle consisted in lowering the temperature of the Peltier at a rate of 1 °C per minute until freezing of the droplet took place. Then temperature was increased to 15 °C and the droplet was left at this temperature for around 10 minutes while complete thawing of the droplet was observed through the optical microscope. Temperature was measured with an accuracy of ±0.1 °C. Experiments were performed in a closed environment with dry N_2 flow inside the Linkam chamber to avoid water condensation from the environment. For exposition to oxygen plasma, the samples were placed in the chamber of a PVA TePla PS210 plasma generator, then the samples were exposed to oxygen plasma (400 W power, 50 SCCM, flow and 200 mTorr of gas pressure) for 20 min. After that, the samples were removed from the

chamber and stored in ambient conditions (temperature range from 20 to 24 °C, relative humidity range from 40 to 60%). Their water freezing capability was measured the same day or a day after plasma exposition. When the effect of water immersion was tested, samples were immersed in MilliQ water for 12 to 48 h and then dried with N_2 before the experiments.

Results

Plots of the nucleation temperatures for 10 consecutive cycles on all pieces cut from the GREEN feldspar are shown in Fig. 2a (GREEN A), Fig. 2b (GREEN B) and Fig. 2c (A and B cuts combined). Each colour in the plot represents a set of experiments of 10 freeze–thaw cycles on a single cut. Circle symbols correspond to experiments performed on pieces cut along the (100) face and star symbols correspond to cuts perpendicular to the (100) face. For all the pieces, the same behaviour was observed; the freezing temperature increases as more cycles are performed until it reaches an approximately constant value (considering the expected dispersion of the freezing temperatures from one cycle to another). This behaviour is observed independently of the direction of the cut (Fig. 2c). We call this behaviour a "history effect" because it seems that the freezing temperature depends on the history of freezing cycles suffered by the sample. The average freezing temperature for each cycle and the dispersion of the values are included in the plot as black squares with error bars.

Differences in the temperatures between the first cycle and the cycles once the freezing temperature is stabilized were in the order of 2 to 5 °C. This behaviour was not reported in published results from other authors with a very similar experimental set-up,[8] where the reported freezing temperatures were scattered around an average value with a dispersion of around 1 to 2 °C. We found a stable freezing behaviour only after a few freeze–thaw cycles were performed (1 to 4 cycles are needed depending on each specific piece). Equivalent plots for the ORANGE and GOLDEN feldspars, displaying the same behaviour as amazonite GREEN feldspar, can be seen in Fig. S3 in the ESI.† However, there is one exception from the rule, where one of the faces of the GOLDEN sample, more precisely the (−201) face, showed almost no history effect up to 10 days after the cut was performed. However, after few months (aged sample) the freezing behaviour worsen, and a history effect appeared (see Fig. S3, ESI†). Nonetheless, once the plasma treatment was applied, this effect vanished. Freezing temperatures obtained when the stable regime was reached were very similar to reported temperatures

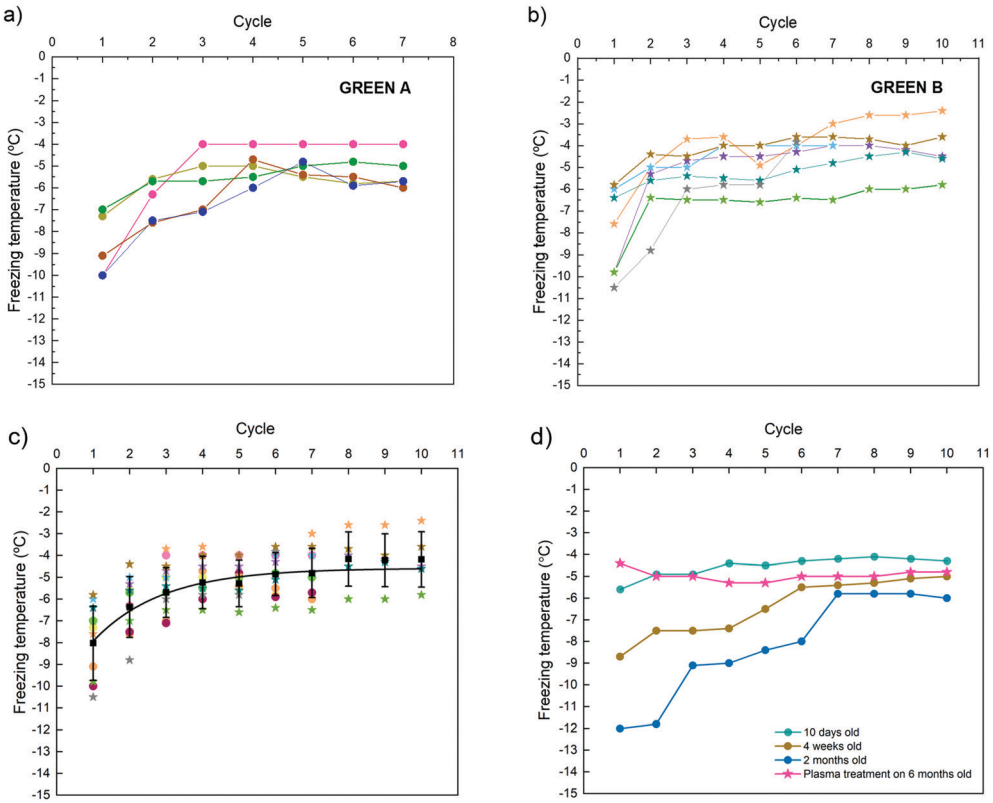

Fig. 2 Freezing temperatures of the water droplet as freeze–thaw cycles are performed on a slide cuts from: (a) the amazonite mineral GREEN A cut (100), (b) the amazonite mineral GREEN B cut; (c) the both cuts: GREEN A (100) – circle symbols and GREEN B – star symbols. Freezing temperature increases until it reaches a stable regime. Each coloured symbol corresponds to a single experiment. Black squares correspond to the average temperature measured from all the experiments shown with error bars indicating standard deviation of the values; (d) variation of the trends observed in (c) with aging of the sample and after exposition of the cut to oxygen plasma. Oxygen plasma treatment induces an almost constant freezing temperature with respect to the freeze–thaw cycle (pink star symbols).

measured on similar minerals,[14,15] including the high efficiency observed on our GOLDEN sample and another sample also obtained from Mt. Malosa.[14]

After the cut, the samples were stored inside a clean box but directly exposed to the air inside the box, thus deposition of dust and particles on the samples is avoided but not the interaction with other molecules in the environment such as humidity and volatile organic compounds (VOCs). Freeze–thaw cycles were repeated after few days, few weeks and after more than a month. Results for one GREEN (100) cut are shown in Fig. 2d, representative of the general trend observed for all the samples upon aging. Measurements performed on samples after few weeks of the cleavage show remarkable variations on the freezing temperatures if compared with measurements performed on samples few days after cleavage. Freezing temperatures for the first freezing event were remarkably lower for the aged samples and the variation between this first freezing temperature and the freezing temperatures when the stable regime was reached was higher than for a fresh sample. Freezing temperatures at the stable regime were usually slightly lower for old samples. If samples were exposed to oxygen plasma, the dependency of the freezing temperature on the cycle disappeared. In those experiments, a droplet of water was deposited on a slide and then 10 freeze–thaw cycles were performed. Immediately after these cycles, the sample was dried with dry N_2 and exposed to oxygen plasma as described in Experimental Section. A new water droplet was deposited, and 10 more cycles were performed. This was observed on both pristine and old samples but in the latter, the effect was dramatic (compare temperatures measured for a two-month-old GREEN sample and after exposing it to oxygen plasma in Fig. 2d).

After plasma exposition, the freezing temperature was approximately constant for all cycles and no history effect was observed. In addition to that, the freezing temperature obtained after plasma exposition was always close to the warmest freezing temperature obtained before plasma exposition and in some cases even a few degrees warmer. In Fig. 3 this effect is summarized for several experiments on each mineral and cut. In this figure we are plotting the percentage of frozen droplets at a given temperature. For example, in Fig. 3a, for the GREEN (100) sample and no plasma treatment, at −6 °C approximately at 70% of the cycles performed, the droplet was already frozen. But, to have 100% of the cycles with frozen droplet, a temperature of −9.1 °C was needed. In contrast to that, for the same sample but

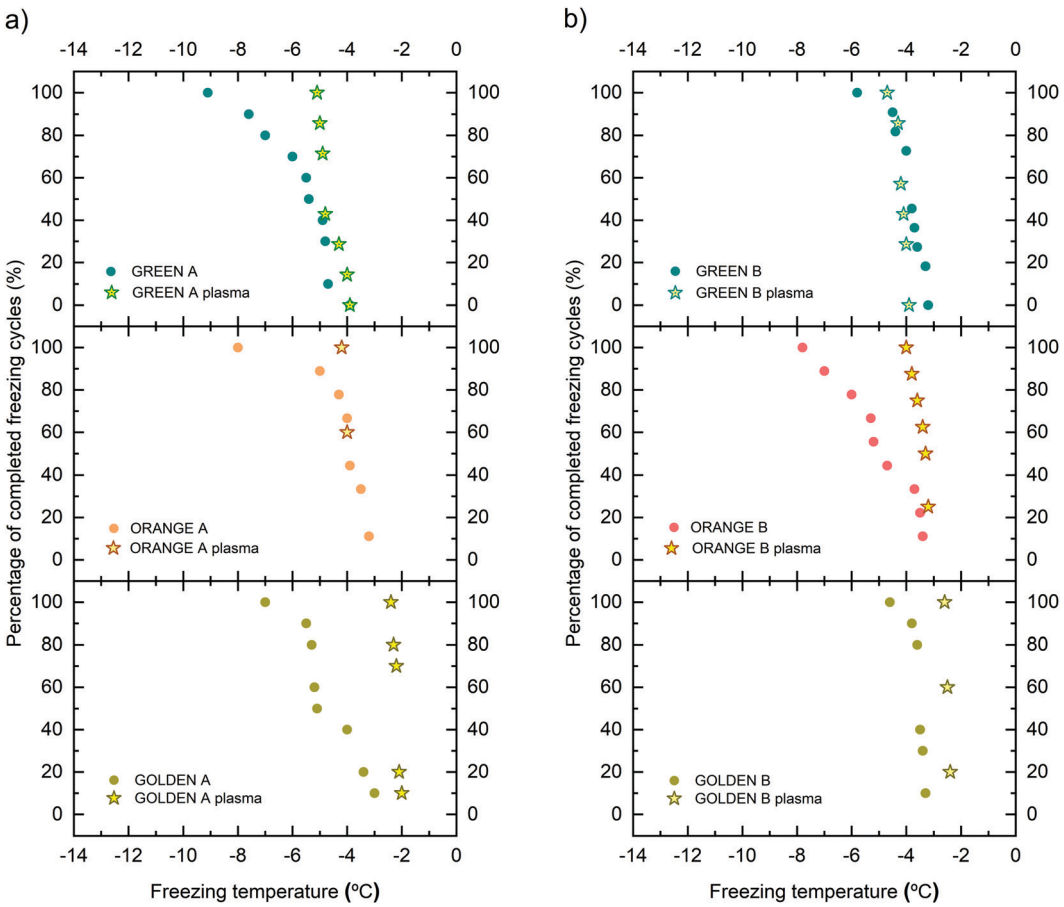

Fig. 3 Percentage of cycles that were already frozen at a given temperature for: GREEN (100) on top left side, GREEN perpendicular cut on top right side, ORANGE (001) on middle left side, ORANGE perpendicular cut on middle right side, GOLDEN (001) on the bottom left side and GOLDEN perpendicular cut on the bottom right side of the figure. Circles represent data for untreated samples and stars represent data from cuts after plasma treatment.

after the plasma treatment, at −5.1 °C 100% of the cycles are completed; meaning 100% of the droplets were already frozen. For the ORANGE A cut after the plasma treatment, 60% of the freezing occurred at −4.0 °C and 100% was concluded already at −4.2 °C, while for the pristine sample the freezing temperatures are much more inhomogeneous showing the spread of freezing temperatures over a wide range between −3.6 °C and −8.0 °C (100%). For the GOLDEN cut B, similar trend was observed, but the effect of the plasma is even more pronounced than for the abovementioned mineral cuts. While for the pristine cut the temperatures spread in the range of −3.0 °C and −7.0 °C (100%), for the plasma treated cut the 10% of the freezing concluded at −2.0 °C and 100% at −2.4 °C, showing a striking difference in ice nucleating capabilities of the later surface. Similar analysis may be done for the other cuts showed in Fig. 3. According to this, two important trends can be observed. First, an increase of the freezing temperate due to the exposition to oxygen plasma was seen in almost all of them (star symbols are at higher temperatures than circle symbols). This indicates that plasma treated surfaces induce IN at higher temperatures than untreated surfaces. Second, the plasma treated surface shows a higher slope in the plot, almost vertical in some cases, indicating that freezing events occur in a narrower range of temperatures than untreated samples, demonstrating a lower dispersion on the freezing temperature values. This is due to the loss of the history effect shown in Fig. 2a. Differences on the efficiency of plasma treatment on different cuts of the same feldspar sample (compare for example GREEN cut A in which plasma is very effective and GREEN cut B) can be explained by differences in OH density on different faces. Different faces can have different oxide density with different reactivity towards water. When those oxides at the surface enter in contact with humidity in ambient air after cleavage, OH groups are formed. Thus, different structures and densities of OH are expected for each face exposed to ambient air. Although, not for the same materials, the formation of surface OH on oxides upon ambient air exposition have been measured by our group using ambient pressure XPS.[25] On the other hand, according to simulations, neither the symmetry of the OH patterns, nor the similarity between a substrate and ice correlated well with the IN ability. Instead, they found that the OH density and the substrate–water interaction strength are useful descriptors of a material's IN ability.[13] So discrepancies in a and b columns of Fig. 3 are probably due to the fact that GREEN B and GOLDEN B cuts are more reactive than A cuts and more OH groups are created on surface oxides when exposed to ambient conditions. Plasma effect on B cuts is minor because there are not a lot of sites able to create new OH groups. The opposite happens for ORANGE.

Samples before and after O_2 plasma treatment were analysed by Scanning Electron Microscopy (SEM) and X-Ray Photoelectron Spectroscopy (XPS). SEM images taken at the same regions of the sample before and after O_2 plasma treatment show that plasma induces morphological changes on the surfaces. Those changes are related to the disappearance of some features on the surface and the appearance of cracks and pores not observed or partially blocked before O_2 plasma exposition (see Fig. 4a). Beyond removal of those features, dimensions of pores seem to be stable after plasma.

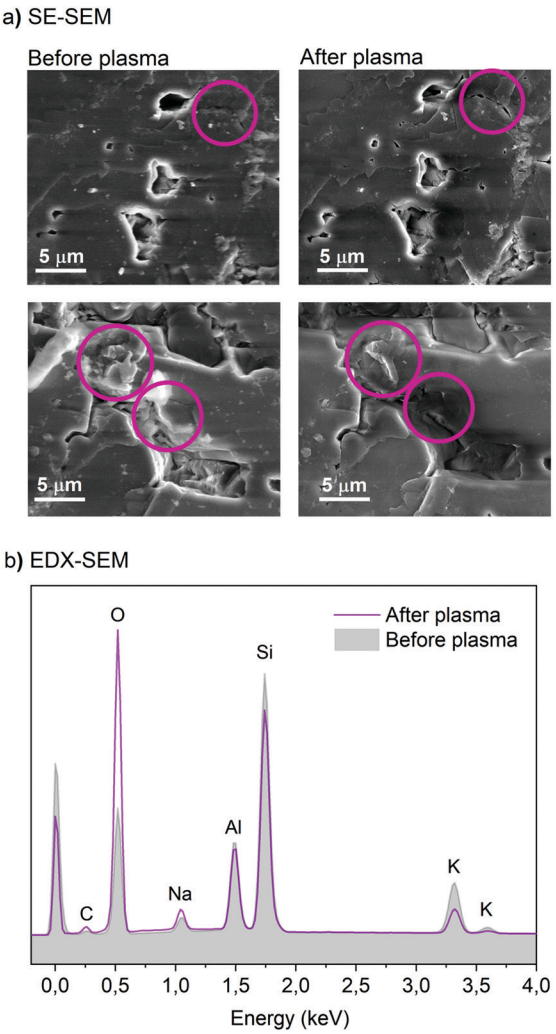

Fig. 4 (a) Secondary electrons SEM (SE-SEM) images of the same areas of feldspar before (left) and after (right) plasma treatment, (b) elemental analysis (EDX spectroscopy) acquired at 10 kV of the area from images showed in (a – top) before (grey area) and after the plasma treatment (pink line). The estimated penetration depth for EDX at 10 kV is less than 1 μm. The purple circles in (a) point out the areas of the surface with substantial morphological changes after plasma exposition.

Elemental distribution maps of the same region showed in Fig. 4a before and after plasma treatment were obtained for different elements: C, Si, O, K, Na, Al (see Fig. S4, ESI†). The maps showed homogeneous intensity on the scanned area for Al, C and Si except for the pores due to the geometry factors resulting in the scattering of electrons at the walls of the pores that reduces the intensity counts for the peaks of all the elements. Oxygen maps show some brighter areas that seem to match areas of high Na intensity. K and Na maps are inverted in intensity between them, indicating areas with more presence of Na at the lattice and other with more presence of K. Maps are not affected by exposition to oxygen plasma except in the case of O that shows an increase in intensity. Quantitative analysis of the relative intensity of each element for the whole image showed a strong increase in the peak associated with oxygen and a reduction of the potassium and silicon peak for the

plasma treated sample. This may be due to a similar process to the well-known weathering of feldspars,[26] in which water alters the feldspar surface by washing out the cations such as K^+ and Na^+ along the H_2SiO_4 by the dissolution of Si into the liquid phase through formation of OH groups on the Si sites. Why only a decrease of potassium and not sodium is observed in this case is unclear. We may speculate, that our samples after being exposed to oxygen plasma and humid air may undergo a similar to weathering process through the formation of surface hydroxyl groups that may cause surface renewal, followed by hydrolysis of Al-O-Si bonds and release of Si from the matrix.[27]

For a better understanding of the effect plasma has on the surface of the studied minerals, high-resolution XPS spectra of O1s, Si2p, Al2p, Na2p, K2p and C1s were acquired before and after O_2 plasma exposition (Fig. 5). Spectra showed a strong reduction of carbon after the treatment, as expected due to the reaction with the organic molecules to produce CO_2. Those organic molecules deposited on the surface as it was exposed to ambient conditions. It has been estimated that after a few hours of exposition to ambient conditions the wetting properties of a surface change dramatically due to the adsorption of such molecules.[28] Two peaks were used to fit O1s spectra, one associated to lattice oxide and another one to surface OH groups, both separated by 0.9 eV, as reported in previous studies of water interaction with different oxides.[25,29,30] From the fittings, it can be clearly observed that the relative ratio between oxides and OH changes after O_2 plasma treatment indicating the formation of OH groups on the surface. Published XPS analysis of Si, SiO_2 and glass after O_2 plasma exposition revealed similar trends in the spectra and were attributed to plasma oxidation of the surface and, when exposed to ambient humidity, an enhanced adsorption of hydroxyls.[31]

Discussion

Minerals, that show an increase in the temperature at which they induce ice-nucleation with successive freeze–thaw cycles, have been proposed in many cases to undergo the pre-activation freezing mechanisms. Those mechanisms are associated with the presence of pores in the minerals.[19,20] SEM images of the samples used in this study revealed the presence of pores on the surface of all samples tested (see Fig. S5 in the ESI†). These pores are characteristic of the specific micro-textures present in alkali feldspar[10,32] and they play a key role as IN sites in feldspars.[8,9,12] The initial freezing spot observed, *i.e.* the nucleation site, was found to be in the vicinity of a surface pore in our samples, as already reported in the literature[8] for similar feldspars. In pore pre-activation mechanism, the ice formed inside the pores in a first IN cycle remains even if conditions of humidity or temperature are changed. The ice inside the pores would induce IN in later freezing cycles at higher temperatures than in the first cycle. Recently, an enhancement of the IN activity of coal fly ash aerosol particles at temperatures up to −10 °C has been observed due to pre-activation at −45 °C.[21]

This pre-activation mechanism is limited at high temperatures, due to the melting of the ice in the pores, and at low relative humidity, due to sublimation from pores. In our experimental

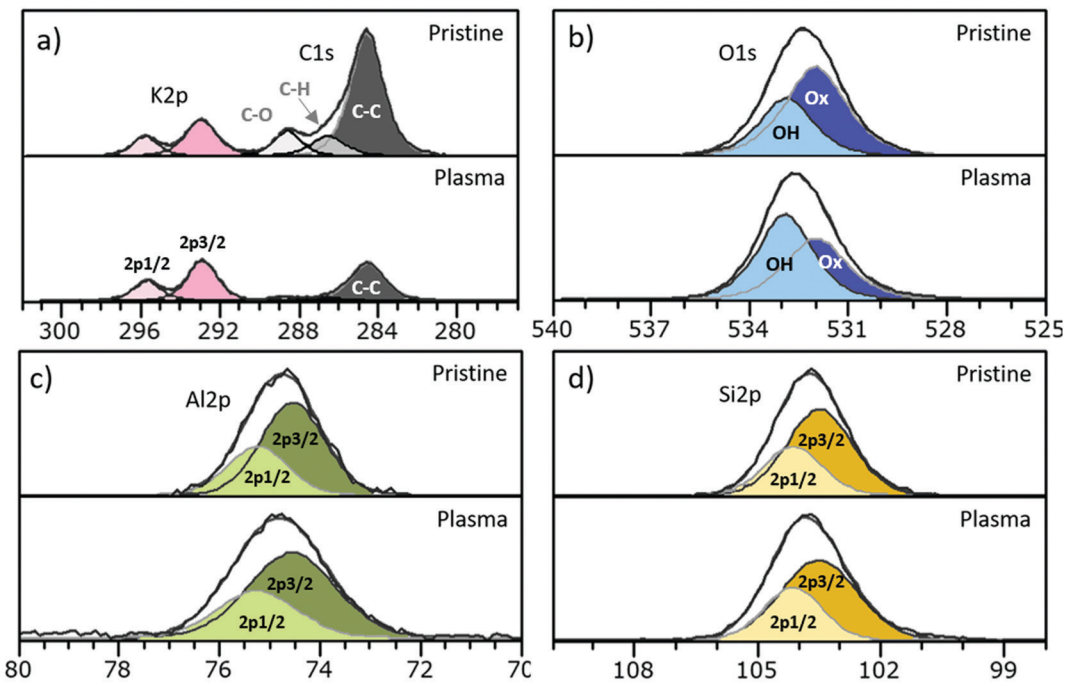

Fig. 5 Fitted X-ray photoelectron spectra (XPS) of GREEN feldspar cuts before and after plasma treatment: (a) C1s and K2p; (b) O1s; (c) Al2p; (d) Si2p. The coloured areas differentiate between peak components; for K2p, Al2p and Si2p between the $2p_{3/2}$ and $2p_{1/2}$, for C1s between 3 components: C–C carbon (adventitious C) in dark grey, C–H carbon in lighter grey and C=O for the lightest tone of grey, for O1s peak we differentiate bulk oxide (Ox) component in dark blue from the OH species (OH) component in light blue.

set–up, where temperature is raised above 0 °C, we do not expect ice to be kept in the micro-sized pores. However, ice (or water in highly structured form) confined in nanometric size features inside pores surviving high temperatures cannot be excluded.[33] Formation of structured ice monolayers was reported several decades ago at organic interfaces.[34] It was later proved that these monolayers may act as pre-activation pathway inducing later freezing cycles at warmer temperatures.[20,35] On minerals, ice-like monolayers at temperatures well above 0 °C have been observed on different materials such as mica,[36] barium fluoride[37] or silicon oxide.[29] Thus, it can be expected that, the ice monolayer formed at the water-feldspar interface inside the pores, could survive to temperatures above 0 °C. However, none of the above mentioned materials, despite having an ice-like monolayer, have been proved to be good ice-nucleating agents.[38,39]

An alternative explanation for pre-activation happening even if temperatures are increased above 0 °C is that a chemical imprint on the OH structure at the surface is left after a freeze–thaw cycle leading to an increase of the IN ability of the surface in following freezing events. This phenomenon has been reported on silica,[16] where it was found that sequential freeze–thaw events induce an increase in the freezing temperature. However, our model to explain the ''history effect'' found in our untreated samples is based on what happens inside the pores. In each freeze–thaw cycle water can penetrate deeper inside the pores because of the volume increase when ice is formed. We consider two possible scenarios that would lead to an increase of IN efficiency when water penetrates deeper into the pores; in a first scenario, water can wet deeper inside the pores when frozen, reaching new IN sites, or in a second scenario expansion of ice could remove some carbon contamination, unblocking pores containing IN sites. While the external part of the pores observed in the SEM images are from hundreds of nanometers to tens of microns we know that the pores can narrow at some points forming ''tunnels'' of sizes below 100 nm.[32,40] Those ''tunnels'' can be of difficult access when water is deposited above the pores. Water can easily form meniscus in those narrow pores not reaching deep IN sites unless the walls of those pores are very hydrophilic. In addition to that, the ''tunnels'' can be blocked by contamination. The volume expansion when water freezes can put water in contact with IN sites not reachable before, this process can take place several times in consecutive cycles until most of the sites are accessible and further cycles would show a stable freezing temperature, as observed in Fig. 2. These two scenarios are schematized in Fig. 6a and b and they could also explain our findings about the feldspars' exposition to oxygen plasma as we describe it in the next paragraph.

On one hand, exposing of silicon oxide surfaces to oxygen plasma is known to increase hydrophilicity of the surface due to the formation of OH groups.[31,41] OH groups are known to play a key role in heterogeneous nucleation,[13] thus the increase and restructuration of surface OH groups can be responsible for the increase of the freezing temperature measured after plasma exposition. The formation of OH groups may create new IN sites on the surface of feldspars and inside the pores, that could

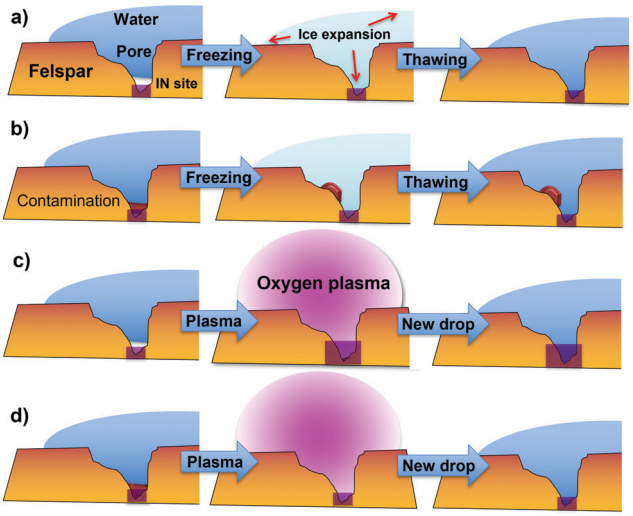

Fig. 6 The mechanisms of freeze–thraw cycles and the plasma treatment on feldspar surfaces: (a) in narrow pores water not always can reach the ice nucleating site but during the expansion of the ice in the first (or following) freezing cycle, water may be able to reach IN site; (b) the possible contamination blocking the IN site may be removed during the freeze–thraw event; (c) the oxygen plasma may enlarge the existing IN site yielding to more active site; (d) oxygen plasma is effective in removing possible carbon related contamination blocking some of the IN sites present on the surface or inside pores of feldspar.

explain the increase in freezing temperature observed after plasma exposition. Plasma can also increase the size of IN sites existing inside pores, making them easier to reach and in this way affect the history effect. These effects are schematized in Fig. 6c. On the other hand, plasma exposition has another important effect on the surface, the reduction of carbon species, *i.e.* the cleaning of the surface that is observed in both XPS and EDX analysis. Carbon species on the surface are not only small molecules scattered randomly on the surface, but they are also present as large clusters of molecules that can block even micro-size pores, as it is observed on SEM images in Fig. 4. Hence, oxygen plasma cleans pores, known to dominate IN,[12] and allows water molecules to reach ice-nucleation sites inside pores, enhancing ice-nucleation efficiency of the minerals (Fig. 6d). Thus, oxygen plasma exposition can produce a similar effect on the feldspar efficiency as IN material to consecutive freeze–thaw events.

It is important to remark that in our measurements we found that plasma has a different impact on freezing temperatures depending on the cut used. In Fig. 3 we can observe that for GREEN, exposition to plasma has an important impact on the A cut (compare dots and stars) while on the B cut it has a minimum impact (dots and stars almost overlap). The opposite happens for the ORANGE sample. These discrepancies are most likely due to the fact that surfaces from different cuts expose different distribution of crystallographic faces and thus they have different density of IN sites, even if they are mostly present in pores only. Since we expect a similar degree of contamination on both cuts, the differences observed might be attributed to the formation of new IN sites on GREEN A and ORANGE B while less IN sites are formed on GREEN B and ORANGE A due to plasma.

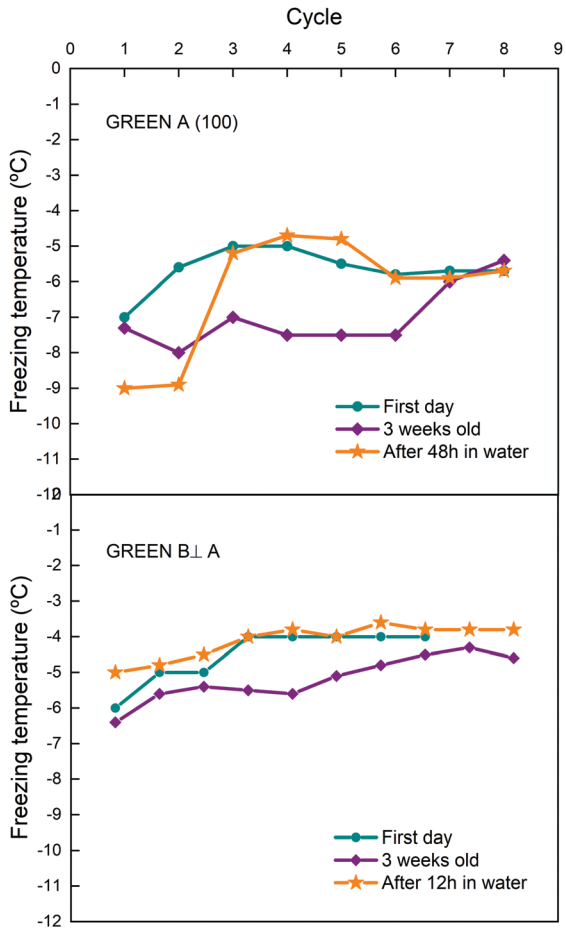

Fig. 7 Effect of water storage on the freezing temperatures of GREEN (100) cut (top) and GREEN B cut (bottom). Green circle symbols represent data acquired on the first day, purple diamond symbols represent data acquired after storage at room conditions for 3 weeks and orange star symbols show data for storage in MiliQ water of aged cuts during 48 h for GREEN A and 12 h for GREEN B.

In our freeze–thaw events we must consider that the feldspar surface is in contact with water for a time that can last in some cases few hours. This can also have an impact on the surface itself; water can remove contaminants from the surface or modify it without the need of freeze–thaw cycles. To gain more insight on that, we tested samples after storage in water for 12 to 48 hours. In Fig. 7 results for two cuts of the GREEN sample are shown where measurements taken the first day after cleavage of the cut, a few weeks later and after immersion in MilliQ water are compared.

On both samples storage in water modifies the behaviour of the freeze–thaw cycles. For GREEN A, a very short history effect is observed after storage in water, and it disappears after three cycles only while seven cycles are needed for the sample stored without water. For GREEN B, a small history effect is observed for 5 cycles but with freezing temperatures higher than before storage. Similar results were observed for other samples, where storage in water can sometimes improve freezing temperatures or lower history effect but a conclusive trend was not observed. However, we may deduce that storage in water probably cleans the surface and facilitates the unblocking of some of the IN sites although it is not as efficient as plasma exposition or performing freeze–thaw cycles. These findings also indicate that the improvement of freezing temperatures with freeze–thaw cycles, *i.e.* the history effect, is due to ice formation on the surface and not to long-term interaction with liquid water. What seems clear from all these findings is that the efficiency of feldspar in inducing IN can be strongly altered by naturally formed organic residues on its surface. These organic residues are mostly formed by volatile organic compounds (VOCs) present in the troposphere and in part emitted by human activity. We can conclude then that feldspar minerals, considered to be the key components of IN dust in mixed clouds,[4] when in contact by VOCs from pollution or natural sources present in the atmosphere can have its activity noticeably reduced.

Conclusions

We have been studying the evolution of the freezing temperature of a water droplet in contact with surfaces of K-feldspars in consecutive freeze–thaw events. We found a general trend where an increase of the freezing temperature is observed during the initial 1 to 4 freezing events and then the freezing temperature remains approximately constant for successive cycles. We call this a "history effect". This effect is more evident for samples aged by exposition to standard room conditions for weeks or months compared to a fresh sample. We observed that after a few cycles (up to 10) the freezing temperatures are similar for fresh and aged samples. This history effect is suppressed if the sample is exposed to oxygen plasma and air. Analysis by XPS and EDX-SEM indicates that exposition to oxygen plasma induces the formation of OH groups on the surface and cleaning from carbon species. Both phenomena enhance the IN ability of the surface and explain the suppression of the history effect. Formation of OH and cleaning of the surface, can also happen during the freeze–thaw cycles explaining the history effect. These findings indicate that the history of feldspar particles in clouds can be an important factor in order to determine their IN activity. In addition, oxygen plasma is revealed as an easy procedure to enhance IN efficiency of feldspar minerals for IN applications.

Conflicts of interest

There are no conflicts to declare.

Acknowledgements

The authors thank C. Marcolli for discussion on results and their interpretation. This work has been supported by the Spanish Government under the project PID2019-110907GB-I00 and the "Severo Ochoa" Program for Centres of Excellence in R&D (CEX2019-000917-S). E. Pach acknowledges the Spanish Ministry of Science and Technology for the Juan de la Cierva Formation grant.

References

1 T. Bartels-Rausch, Ten things we need to know about ice and snow, *Nature*, 2013, **494**, 27–29.
2 V. F. Petrenko and R. W. Whitworth, *Physics of Ice*, Oxford University Press, 2002.
3 Z. A. Kanji, L. A. Ladino, H. Wex, Y. Boose, M. Burkert-Kohn, D. J. Cziczo and M. Krämer, Overview of ice nucleating particles, *Meteorol. Monogr.*, 2017, **58**, 1.1–1.33.
4 J. D. Atkinson, B. J. Murray, M. T. Woodhouse, T. F. Whale, K. J. Baustian, K. S. Carslaw, S. Dobbie, D. O'Sullivan and T. L. Malkin, The importance of feldspar for ice nucleation by mineral dust in mixed-phase clouds, *Nature*, 2013, **498**, 355–358.
5 C. Marcolli, Technical note: Fundamental aspects of ice nucleation *via* pore condensation and freezing including Laplace pressure and growth into macroscopic ice, *Atmos. Chem. Phys.*, 2020, **20**, 3209–3230.
6 L. Kaufmann, C. Marcolli, B. Luo and T. Peter, Refreeze experiments with water droplets containing different types of ice nuclei interpreted by classical nucleation theory, *Atmos. Chem. Phys.*, 2017, **17**, 3525–3552.
7 R. O. David, C. Marcolli, J. Fahrni, Y. Qiu, Y. A. Perez Sirkin, V. Molinero, F. Mahrt, D. Brühwiler, U. Lohmann and Z. A. Kanji, Pore condensation and freezing is responsible for ice formation below water saturation for porous particles, *Proc. Natl. Acad. Sci. U. S. A.*, 2019, **116**, 8184–8189.
8 M. A. Holden, T. F. Whale, M. D. Tarn, D. O'Sullivan, R. D. Walshaw, B. J. Murray, F. C. Meldrum and H. K. Christenson, High-speed imaging of ice nucleation in water proves the existence of active sites, *Sci. Adv.*, 2019, **5**, eaav4316.
9 A. Kiselev, F. Bachmann, P. Pedevilla, S. J. Cox, A. Michaelides, D. Gerthsen and T. Leisner, Active sites in heterogeneous ice nucleation-the example of K-rich feldspars, *Science*, 2017, **355**, 367–371.
10 F. D. L. Walker, M. R. Lee and I. Parsons, Micropores and micropermeable texture in alkali feldspars: Geochemical and geophysical implications, *Mineral. Mag.*, 1995, **59**, 505–534.
11 T. F. Whale, M. A. Holden, A. N. Kulak, Y.-Y. Kim, F. C. Meldrum, H. K. Christenson and B. J. Murray, The role of phase separation and related topography in the exceptional ice-nucleating ability of alkali feldspars, *Phys. Chem. Chem. Phys.*, 2017, **19**, 31186–31193.
12 E. Pach and A. Verdaguer, Pores dominate ice nucleation on feldspars, *J. Phys. Chem. C*, 2019, **123**, 20998–21004.
13 P. Pedevilla, M. Fitzner and A. Michaelides, What makes a good descriptor for heterogeneous ice nucleation on OH-patterned surfaces, *Phys. Rev. B*, 2017, **96**, 115441.
14 A. D. Harrison, T. F. Whale, M. A. Carpenter, M. A. Holden, L. Neve, D. O'Sullivan, J. Vergara Temprado and B. J. Murray, Not all feldspars are equal: A survey of ice nucleating properties across the feldspar group of minerals, *Atmos. Chem. Phys.*, 2016, **16**, 10927–10940.
15 A. Peckhaus, A. Kiselev, T. Hiron, M. Ebert and T. Leisner, A comparative study of K-rich and Na/Ca-rich feldspar ice-nucleating particles in a nanoliter droplet freezing assay, *Atmos. Chem. Phys.*, 2016, **16**, 11477–11496.
16 A. Abdelmonem, S. Ratnayake, J. D. Toner and J. Lützenkirchen, Cloud history can change water–ice–surface interactions of oxide mineral aerosols: a case study on silica, *Atmos. Chem. Phys.*, 2020, **20**, 1075–1087.
17 G. R. Edwards, L. F. Evans and A. F. Zippear, Two-dimensional phase changes in water adsorbed on ice-nucleating substrates, *Trans. Faraday Soc.*, 1970, **66**, 220–234.
18 R. A. Shaw, A. J. Durant and Y. Mi, Heterogeneous surface crystallization observed in undercooled water, *J. Phys. Chem. B*, 2005, **109**, 9865–9868.
19 R. Wagner, A. Kiselev, O. Möhler, H. Saathoff and I. Steinke, Pre-activation of ice-nucleating particles by the pore condensation and freezing mechanism, *Atmos. Chem. Phys.*, 2016, **16**, 2025–2042.
20 C. Marcolli, Pre-activation of aerosol particles by ice preserved in pores, *Atmos. Chem. Phys.*, 2017, **17**, 1595–1622.
21 N. S. Umo, R. Wagner, R. Ullrich, A. Kiselev, H. Saathoff, P. G. Weidler, D. J. Cziczo, T. Leisner and O. Möhler, Enhanced ice nucleation activity of coal fly ash aerosol particles initiated by ice-filled pores, *Atmos. Chem. Phys.*, 2019, **19**, 8783–8800.
22 A. Kiselev, A. Keinert, T. Gaedecke, T. Leisner, C. Sutter, E. Petrishcheva and R. Abart, Effect of chemically induced fracturing on the ice nucleation activity of alkali feldspar, *Atmos. Chem. Phys.*, 2021, 1–17.
23 E. Pach, L. Rodriguez and A. Verdaguer, Substrate dependence of the freezing dynamics of supercooled water films: A high-speed optical microscope study, *J. Phys. Chem. B*, 2018, **122**(2), 818–826.
24 M. Ostrooumov, *Amazonite. Mineralogy, Crystal Chemistry and Typomorphism*, Elsevier, 2016.
25 N. Domingo, E. Pach, K. Cordero-Edwards, V. Pérez-Dieste, C. Escudero and A. Verdaguer, Water adsorption, dissociation and oxidation on SrTiO3 and ferroelectric surfaces revealed by ambient pressure X-ray photoelectron spectroscopy, *Phys. Chem. Chem. Phys.*, 2019, **21**, 4920–4930.
26 G. Yuan, Y. Cao, H.-M. Schulz, F. Hao, J. Gluyas, K. Liu, T. Yang, Y. Wang, K. Xi and F. Li, A review of feldspar alteration and its geological significance in sedimentary basins: From shallow aquifers to deep hydrocarbon reservoirs, *Earth-Sci. Rev.*, 2019, **191**, 114–140.
27 Y. Yang, Y. Min, J. Lococo and Y.-S. Jun, Effects of Al/Si ordering on feldspar dissolution: Part I. Crystallographic control on the stoichiometry of dissolution reaction, *Geochim. Cosmochim. Acta*, 2014, **126**, 574–594.
28 C. A. Amadei, C.-Y. Lai, D. Heskes and M. Chiesa, Time dependent wettability of graphite upon ambient exposure: The role of water adsorption, *J. Chem. Phys.*, 2014, **141**, DOI: 10.1063/1.4893711.
29 A. Verdaguer, C. Weis, G. Oncins, G. Ketteler, H. Bluhm and M. Salmero, Growth and structure of water on SiO_2 films on Si investigated by kelvin probe microscopy and *in situ* X-ray spectroscopies, *Langmuir*, 2007, **23**, 9699–9703.
30 K. Cordero-Edwards, L. Rodríguez, A. Calò, M. J. Esplandiu, V. Pérez-Dieste, C. Escudero, N. Domingo and A. Verdaguer,

Water affinity and surface charging at the z-Cut and y-Cut $LiNbO_3$ surfaces: An ambient pressure X-ray photoelectron spectroscopy study, *J. Phys. Chem. C*, 2016, **120**, 24048–24055.

31 A. U. Alam, M. M. R. Howlader and M. J. Deen, The effects of oxygen plasma and humidity on surface roughness, water contact angle and hardness of silicon, silicon dioxide and glass, *J. Micromech. Microeng.*, 2014, **24**, 035010.

32 J. D. F. Gerald, I. Parsons and N. Cayzer, Nanotunnels and pull-aparts: Defects of exsolution lamellae in alkali feldspars, *Am. Mineral.*, 2006, **91**, 772–783.

33 A. Verdaguer, J. J. Segura, L. López-Mir, G. Sauthier and J. Fraxedas, *J. Chem. Phys.*, 2013, **138**, 121101.

34 L. F. Evans, Two-dimensional nucleation of ice, *Nature*, 1967, **213**, 384–385.

35 L. H. Seeley and G. T. Seidler, Preactivation in the nucleation of ice by Langmuir films of aliphatic alcohols, *J. Chem. Phys.*, 2001, **114**, 10464–10470.

36 T. K. Shimizu, S. Maier, A. Verdaguer, J. J. Velasco-Velez and M. Salmeron, *Prog. Surf. Sci.*, 2018, **93**, 87–107.

37 A. Verdaguer, M. Cardellach and J. Fraxedas, Thin water films grown at ambient conditions on $BaF_2(111)$ studied by scanning polarization force microscopy, *J. Chem. Phys.*, 2008, **129**, 174705.

38 P. Conrad, G. E. Ewing, R. L. Karlinsey and V. Sadtchenko, Ice nucleation on $BaF_2(111)$, *J. Chem. Phys.*, 2005, **122**, DOI: 10.1063/1.1844393.

39 A. Kumar, C. Marcolli and T. Peter, Ice nucleation activity of silicates and aluminosilicates in pure water and aqueous solutions-Part 3: Aluminosilicates, *Atmos. Chem. Phys.*, 2019, **19**, 6059–6084.

40 E. Pach and A. Verdaguer, Pores dominate ice nucleation on feldspars, *J. Phys. Chem. C*, 2019, **123**, 20998–21004.

41 A. U. Alam, M. M. R. Howlader and M. J. Deen, Oxygen plasma and humidity dependent surface analysis of silicon, silicon dioxide and glass for direct wafer bonding, *ECS J. Solid State Sci. Technol.*, 2013, **2**, P515–P523.

